

Ateneo de Manila University

Archium Ateneo

Physics Faculty Publications

Physics Department

2020

An annual time series of weekly size-resolved aerosol properties in the megacity of Metro Manila, Philippines

Connor Stahl

Melliza Templonuevo Cruz

Paola Angela Bañaga

GRACE BETITO

Rachel A. Braun

See next page for additional authors

Follow this and additional works at: <https://archium.ateneo.edu/physics-faculty-pubs>



Part of the [Atmospheric Sciences Commons](#), and the [Physical Chemistry Commons](#)

Authors

Connor Stahl, Melliza Templonuevo Cruz, Paola Angela Bañaga, GRACE BETITO, Rachel A. Braun, Mojtaba Azadi Aghdam, Maria Obiminda L. Cambaliza, Genevieve Rose Lorenzo, Alexander B. MacDonald, Preciosa Corazon Pabroa, John Robin Yee, James Bernard Simpás, and Armin Sorooshian



OPEN

DATA DESCRIPTOR

An annual time series of weekly size-resolved aerosol properties in the megacity of Metro Manila, Philippines

Connor Stahl¹, Melliza Templonuevo Cruz^{2,3}, Paola Angela Bañaga^{2,4}, Grace Betito^{2,4}, Rachel A. Braun¹, Mojtaba Azadi Aghdam¹, Maria Obiminda Cambaliza^{2,4}, Genevieve Rose Lorenzo^{2,5}, Alexander B. MacDonald¹, Preciosa Corazon Pabroa⁶, John Robin Yee⁶, James Bernard Simpás^{2,4} & Armin Sorooshian^{1,5}✉

Size-resolved aerosol samples were collected in Metro Manila between July 2018 and October 2019. Two Micro-Orifice Uniform Deposit Impactors (MOUDI) were deployed at Manila Observatory in Quezon City, Metro Manila with samples collected on a weekly basis for water-soluble speciation and mass quantification. Additional sets were collected for gravimetric and black carbon analysis, including during special events such as holidays. The unique aspect of the presented data is a year-long record with weekly frequency of size-resolved aerosol composition in a highly populated megacity where there is a lack of measurements. The data are suitable for research to understand the sources, evolution, and fate of atmospheric aerosols, as well as studies focusing on phenomena such as aerosol-cloud-precipitation-meteorology interactions, regional climate, boundary layer processes, and health effects. The dataset can be used to initialize, validate, and/or improve models and remote sensing algorithms.

Background & Summary

The composition and size distribution of ambient particulate matter (PM) influence how particles impact air quality and public health¹, climate², the hydrological cycle³, and geochemical cycling of nutrients and contaminants⁴. Depending on particle size and composition, an inhaled particle can deposit in the extrathoracic (head), tracheobronchial (TB), or pulmonary (PUL) regions, which can have serious implications for health^{5–8}. Similarly, size and composition of particles impact their radiative properties, ability to act as cloud condensation nuclei (CCN), and also the ability to be transported between regions.

Since seasonal changes in meteorology, transport pathways, and emissions can impact a given region, annual PM cycles are important to characterize. A summary of past long-term (> three-month period) size-resolved PM substrate-based sampling efforts are provided in Online-only Table 1. There are a scarcity of annual time series data with at least weekly frequency regardless of global region. Most substrate-based sampling efforts for size-fractionated PM cover periods of one to three months with a sample collection duration between 24 to 96 hours per set, which were not included in Online-only Table 1. Longer sampling periods for individual sets, reaching up to a week^{9,10}, are required in regions with less pollution in order to achieve sufficiently high mass concentrations (i.e. above limits of detection) for targeted species. The difficulty in obtaining long-term records of size-resolved PM composition with high temporal frequency is largely due to the labor-intensive nature of such measurements, which include several pre- and post- sampling steps and subsequent chemical analyses.

The megacity of Metro Manila in the Philippines consists of 16 cities containing approximately 12.88 million people, with a collective population density of about 20,800 km⁻²^{11,12}. Quezon City, the location where sampling

¹Department of Chemical and Environmental Engineering, University of Arizona, Tucson, Arizona, USA. ²Manila Observatory, Quezon City, 1108, Philippines. ³Institute of Environmental Science and Meteorology, University of the Philippines, Diliman, Quezon City, 1101, Philippines. ⁴Department of Physics, School of Science and Engineering, Ateneo de Manila University, Quezon City, 1108, Philippines. ⁵Department of Hydrology and Atmospheric Sciences, University of Arizona, Tucson, Arizona, USA. ⁶Department of Science and Technology, Philippine Nuclear Research Institute, Commonwealth Avenue, Diliman, Quezon City, 1101, Philippines. ✉e-mail: armin@email.arizona.edu

Instrument	Parameters
Aerosol Robotic Network (AERONET)	Aerosol optical depth (AOD), single-scatter albedo (SSA), absorption angstrom exponent (AAE), scattering angstrom exponent (SAE), and water vapor
Disdrometer	Droplet size and vertical velocity
Arctic High Spectral Resolution Lidar (AHSRL)	Backscatter coefficient, depolarization ratio, and backscatter ratio
DustTrak and (2) Tactical Air Samplers (TAS)	Real-time and 24-hour total PM _{2.5} mass concentration with chemical speciation
Solar Spectral Flux Radiometer (SSFR)	Shortwave and longwave radiance and irradiance
All-Sky Camera	Hemispheric sky imaging
Particle Soot Absorption Photometer (PSAP)	Black carbon absorption and concentration
Automated Weather Station (AWS)	Temperature, relative humidity, wind speed, wind direction, solar radiation, pressure, and precipitation
Davis Rotation Uniform-Cut Monitor (DRUM)	Size segregated elemental composition of PM
Electronic Beta Attenuation Monitor (e-BAM)	Real-time PM _{2.5} mass concentration
Kipp and Zonen CMP22 Pyranometer	Solar radiation (broadband irradiance)
Kipp and Zonen CGR4 Pyrgeometer	Solar radiation (infrared irradiance)
SPN1 Shadow Pyranometer	Solar radiation (shadow broadband irradiance)
SP1-F Narrowband Shadow Pyranometer	Solar radiation (shadow narrowband irradiance)

Table 1. List of instruments deployed at Manila Observatory (MO) before and during CAMP² Ex and the associated measurement parameters.

took place, is one of the most populated cities in the region, with a population of about 2.94 million people and a population density of approximately 17,000 km⁻²¹², which is among the highest in the world. Metro Manila is an ideal location for examining locally produced urban anthropogenic PM often mixed with a host of other air masses of marine and continental origin that are transported over both short and long distances to Metro Manila¹³. One aspect that makes the PM in Metro Manila unique is that black carbon levels are among the highest in the world^{11,14,15}. The elevated black carbon is mainly due to vehicular emissions, more specifically the jeepneys, large trucks, and outdated vehicles¹¹. The Philippines serves as a representative southeastern Asian country in terms of high population density, rapid urbanization, outdated vehicle usage and technology, and more lenient air regulations¹¹.

The goal of this work is to present a 16-month size-resolved PM dataset for Metro Manila, Philippines. The unique geographic position of Metro Manila coupled to the wide ranging meteorology and transport patterns makes this dataset highly valuable in terms of examining numerous topics related to PM physics and chemistry with general implications for other regions: (i) impacts of PM on regional climate, clouds, and monsoonal activity, (ii) PM removal via wet deposition, (iii) aqueous processing of PM, (iv) source apportionment, (v) effects on PM properties due to mixing of varying air masses, (vi) catalytic and destructive effects of metals on inorganic/organic species, (vii) impacts of extreme events (e.g., biomass burning, dust storms, fireworks, typhoons) on regional PM, and (viii) public health implications.

Methods

Field study description. The dataset presented is a 16-month, size-resolved, chemical characterization of PM as part of a pre-campaign initiative for the Cloud, Aerosol, and Monsoon Processes Philippines Experiment (CAMP²Ex) titled CAMP²Ex weatHER and CompoSition Monitoring (CHECSM) study. The CHECSM campaign took place between July 2018 through October 2019, within which August through October 2019 coincides with the airborne component of CAMP²Ex.

Study site description. The CHECSM study occurred at the Manila Observatory (MO; 14.64°N, 121.08°E) located at the Ateneo de Manila campus in Quezon City, Philippines. The site was segregated from surrounding urban areas, including a major roadway, by a grove of trees circling the campus. However, it was clearly impacted by local urban emissions and long-range transport based on results from the first six months of data collected^{16–18}. Sampling took place on the 3rd floor of the MO office building, which was approximately 85 m above sea level. Figure 1 shows a timeline of sampling, which occurred in four identified seasons: the 2018 southwest monsoon/wet season (18 June–4 October)^{19,20}, a transitional period (5–25 October), the northeast monsoon/dry season (26 October 2018–10 June 2019)²¹, and the 2019 southwest monsoon/wet season (11 June–7 October)^{22,23}. The southwest monsoon is characterized by relatively high temperatures, high humidity, frequent and heavy rainfall, and winds coming predominantly from the southwest. The northeast monsoon is characterized by moderate rainfall, low humidity, lower temperatures, and winds affecting the eastern side of the country. The characteristics of the monsoons listed above are general traits, but the major determining factor is rainfall. The measured temperature, humidity, and rainfall during sampling period collected at MO ranged from 25.4–30.2 and 24.2–30.9 °C, 59–94 and 54–85%, and 0–78.4 and 0–32.6 mm for the southwest and northeast monsoons, respectively, with average values of 27.6 and 27.7 °C, 72 and 64%, and 18.8 and 2.1 mm. Although the focus of this data descriptor is the size-resolved PM composition dataset, additional instrumentation co-located at MO during CHECSM is summarized in Table 1.

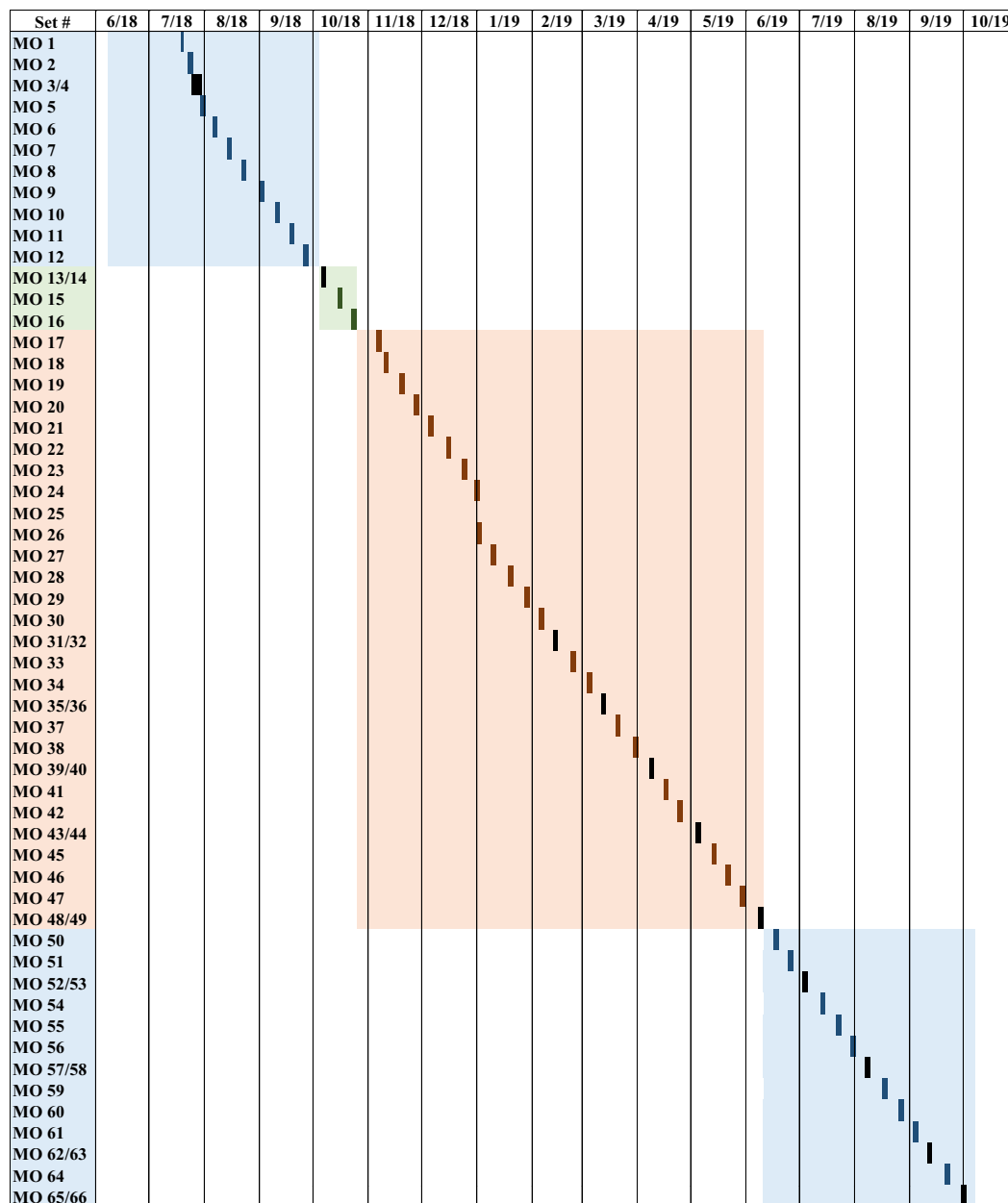


Fig. 1 Timeline of size-resolved aerosol measurements at the Manila Observatory. Light blue boxes represent the southwest monsoon/wet seasons, the light green box represents the transitional period, and the orange box represents the northeast monsoon/dry season. Dark colored boxes represent MOUDI sampling periods and black boxes represent parallel MOUDI sampling periods.

Instrument description. Size-resolved PM was collected using a pair of Micro-Orifice Uniform Deposit Impactors II (MOUDI II 120 R, MSP Corporation, Marple *et al.*²⁴) on Teflon substrate filters (PTFE membrane, 2 μm pores, 46.2 mm diameter, Whatman). The MOUDI-II is a 10-stage impactor with aerodynamic cutpoint diameters (D_p) of 10, 5.6, 3.2, 1.8, 1.0, 0.56, 0.32, 0.18, 0.10, and 0.056 μm with a pre-impactor ($> 18 \mu\text{m}$) and an after-filter ($< 0.056 \mu\text{m}$). Refer to Table 2 for the associated stage numbers, collected diameter ranges, and cutpoint diameters. The instruments operated at a nominal flowrate of $\sim 30 \text{ L min}^{-1}$, with measured flowrates for each set reported in Table 3. Each stage, except for the pre-impactor and after-filter, continuously rotates to allow for uniform deposition of particles. Pressures for each stage were measured and recorded to ensure pressure drops were within acceptable ranges. An identical pair of MOUDIs were deployed for two reasons: (i) there would be no delay in sampling when a unit required maintenance, and (ii) simultaneous measurements allowed for additional analyses of collected PM.

MOUDI sets were collected weekly over a 48-hour period with the exception of sets MO1, MO2, MO3/4, MO5, MO31/32, and MO51, which were collected for 24, 54, 119, 42, 49, and 50 hours, respectively. MOUDI sets labeled MO#/# refer to the sets that were simultaneously collected so that both chemical analysis and

Stage #	Diameter Range (μm)	Cutpoint Diameter (μm)
1	> 18	18
2	18–10	10
3	10–5.6	5.6
4	5.6–3.2	3.2
5	3.2–1.8	1.8
6	1.8–1.0	1.0
7	1.0–0.56	0.56
8	0.56–0.32	0.32
9	0.32–0.18	0.18
10	0.18–0.10	0.10
11	0.10–0.056	0.056
12	< 0.056	< 0.056

Table 2. List of the stages and the respective collected diameter range and cutpoint diameters.

gravimetric analysis could be performed. A total of 66 sets were collected; 11 of the sets were collected using the simultaneous sampling approach, 54 of the sets were analyzed using ion chromatography (IC; Thermo Scientific Dionex ICS-2100 system), 47 of the sets were also analyzed using triple quadrupole inductively coupled plasma mass spectrometry (ICP-QQQ; Agilent 8800 Series), and 1 set (MO25) was collected as a special microscopy set. Additional MOUDI sets were collected on aluminum substrates for microscopy analysis using a Scanning Electron Microscope (SEM); however, these sets are not included in the dataset presented here. For more information on these sets, please refer to Cruz *et al.*¹⁶.

The MOUDIs were set up in such a way to reduce both particle losses and blockage of the inlet. The inlet tubing connecting the MOUDI to ambient air was constructed of stainless steel. The tubing was bent meticulously with a large radius such that there were no kinks. The inlet of the tubing was oriented downwards to prevent water from entering the MOUDI. To further avoid debris from getting into the inlet, a funnel with a mesh covering was attached securely to the downward facing tube opening exposed to ambient air. The temperature differential between the outside air and the tubing was either negligible or the tubing was slightly warmer than the outside air, thus reducing the possibility of thermal deposition. As the average relative humidity measured onsite over the sampling period was approximately 68% ranging from 54–94% throughout the year, the diameters of sampled particles correspond to wet rather than dry diameters and particle bounce was not significant²⁵. This is additionally supported by particle morphology characterization showing evidence of halo areas, indicative of the particles being saturated when impacting onto the substrates^{26–28}, surrounding particles in both the fine and coarse size ranges^{16,17}.

Pre-Sampling processing. The Teflon substrates were prepared prior to use by soaking each substrate face for a minimum of 12 hours in ~7.6 cm of Milli-Q (18.2 M Ω -cm) water in a laminar flow hood and/or covered container. Once each substrate face was soaked, the substrates were removed and placed in methanol cleaned Petrislides (Millipore), which were left slightly open in a laminar flow hood to dry any water residue. Once the substrates were dry, the Petrislides were closed and sealed using Parafilm to ensure the substrates were devoid of any particles or gases that could deposit on them.

Post-Sampling processing. Figure 2 summarizes the post-sampling process to reach the final dataset. After sampling was completed, substrates were first cut in half using ceramic scissors so one-half could be used for extraction in Milli-Q water and the other half could be stored in a freezer at $-20\text{ }^{\circ}\text{C}$ for future analyses. Ceramic scissors that were cleaned with methanol were used to cut the substrates in half in order to prevent contamination of heavy metals from other cutting instruments (e.g. metal scissors). The ceramic scissors were subsequently cleaned with methanol after each cut. Substrate extractions were performed using 8 mL of Milli-Q water (18.2 M Ω -cm) in cleaned 15 mL polypropylene centrifuge tubes that were sonicated for 30 minutes at 25–30 $^{\circ}\text{C}$. Samples were extracted in this temperature range to ensure all targeted organics would solubilize. Additionally, during sampling, temperatures ranged from 28.7–45.7 $^{\circ}\text{C}$; therefore, any volatile species were expected to be gone prior to the point of sampling and well before extractions took place. There have been other papers that performed similar extractions with temperatures up to 60 $^{\circ}\text{C}$ ^{29–33}. Sonicated solutions were then decanted into two different containers for analysis: (i) 0.5 mL polypropylene vial with a filter cap for analysis via IC, and (ii) a polypropylene centrifuge tube for analysis via ICP-QQQ. The remainder of the solutions were then stored in a refrigerator at 0 $^{\circ}\text{C}$. Blank substrates were also processed in a similar manner to serve as background control samples. The motivation behind using water for extractions was owing to the importance of the results for health effects and toxicological studies, radiative effects, atmospheric residence time, nucleation efficiency, and bioavailability^{34–39}.

Ions. Cationic and anionic water-soluble PM speciation and quantification was conducted using a 2 mm IC system at a flowrate of 0.4 mL min⁻¹. The cationic species measured were Na⁺, NH₄⁺, Mg²⁺, Ca²⁺, dimethylamine (DMA), trimethylamine (TMA), and diethylamine (DEA) using an eluent of methanesulfonic acid. The anionic species measured were methanesulfonate (MSA), pyruvate, adipate, succinate, maleate, oxalate, phthalate, Cl⁻,

Sample ID	Avg. Flow (L/min)	Run Time (hr)	Avg. Temp. (°C)	Avg. RH (%)	Days of the Week	Sample ID	Avg. Flow (L/min)	Run Time (hr)	Avg. Temp. (°C)	Avg. RH (%)	Days of the Week
MO1	29.6	24	30.5	59.0	Th-F	MO34	29.4	48	35.3	57.9	M-W
MO2	29.6	54	31.7	66.8	M-W	MO35 (G)	25.6	48	36.6	56.8	T-Th
MO3 (G)	28.6	119	34.9	69.0	W-M	MO36	29.3	48	39.9	56.8	T-Th
MO4	30.3	119	34.4	69.0	W-M	MO37	30.0	48	38.8	55.1	W-F
MO5	28.8	42	33.5	66.7	M-W	MO38	29.6	48	36.4	54.0	S-M
MO6	27.1	48	34.6	63.3	M-W	MO39 (G)	26.4	48	39.0	57.6	M-W
MO7	27.9	48	34.9	78.3	T-Th	MO40	29.6	48	41.4	57.6	M-W
MO8	29.0	48	35.7	78.2	W-F	MO41	29.1	48	38.7	57.7	T-Th
MO9	27.5	48	34.9	68.4	S-M	MO42	29.1	48	40.3	53.7	W-F
MO10	29.0	48	36.7	65.2	M-W	MO43 (G)	26.8	48	36.1	59.8	S-M
MO11	27.1	48	35.8	68.3	T-Th	MO44	28.6	48	37.0	59.8	S-M
MO12	27.5	48	37.0	70.9	W-F	MO45	28.7	48	37.3	61.8	M-W
MO13 (G)	29.8	48	35.1	73.1	S-M	MO46	28.7	48	39.0	72.2	T-Th
MO14	26.1	48	32.0	73.1	S-M	MO47	28.9	48	39.3	64.5	W-F
MO15	29.7	48	37.3	67.6	M-W	MO48	28.0	48	38.9	62.6	S-M
MO16	29.2	48	37.6	67.7	T-Th	MO49 (G)	25.5	48	38.1	62.6	S-M
MO17	30.0	48	36.5	60.6	W-F	MO50	28.8	48	39.2	64.4	M-W
MO18	29.5	48	36.7	61.9	S-M	MO51	27.8	50	36.2	77.1	T-Th
MO19	31.4	48	35.8	61.4	M-W	MO52 (G)	24.9	48	36.6	60.9	W-F
MO20	30.2	48	34.8	60.8	T-Th	MO53	26.9	48	38.8	60.9	W-F
MO21	30.5	48	34.8	72.0	W-F	MO54	28.8	48	36.8	66.4	S-M
MO22	29.6	48	32.7	78.5	S-M	MO55	28.8	48	38.0	75.4	M-W
MO23	26.4	48	29.7	81.8	M-W	MO56	26.7	48	35.0	76.1	T-Th
MO24	30.2	48	35.8	84.6	M-W	MO57	27.5	48	33.0	94.1	W-F
MO25 (AL)	N/A	2.75	N/A	N/A	M-T	MO58 (G)	24.5	48	33.4	94.1	W-F
MO26	24.1	48	35.0	77.2	T-Th	MO59	28.2	48	37.8	85.9	S-M
MO27	23.9	48	36.2	65.3	W-F	MO60	28.2	48	37.3	92.7	M-W
MO28	25.0	48	33.1	63.5	S-M	MO61	29.4	48	36.3	62.1	T-Th
MO29	29.5	48	34.5	63.3	M-W	MO62	27.8	48	36.5	77.0	W-F
MO30	29.8	48	34.4	60.7	T-Th	MO63 (G)	24.4	48	35.0	77.0	W-F
MO31	29.9	49	35.8	65.7	W-F	MO64	27.0	48	37.5	67.2	S-M
MO32 (G)	24.4	49	37.0	65.7	W-F	MO65	27.2	48	38.4	65.3	M-W
MO33	29.8	48	34.3	58.1	S-M	MO66 (G)	23.9	48	37.7	57.9	M-W

Table 3. MOUDI sample set operating data. The table includes average flowrates, total sample run time, average operating temperature of the MOUDI cabinet, relative humidity (RH), and the days of the week sampling occurred. The start/end times varied between 13:00 and 15:00 local time for standard sets and 5:00 local time for dual gravimetric/IC sets. Sets with a label of (G) are gravimetric sets and the set labeled (AL) was collected for SEM analysis. All other sets were only measured with IC and/or ICP-QQQ.

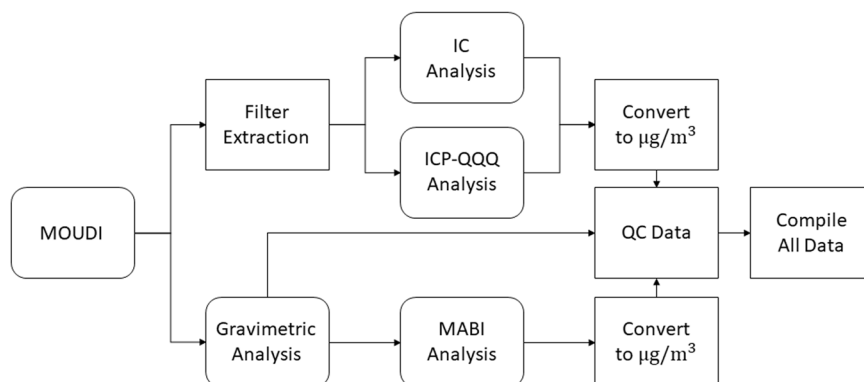


Fig. 2 Flow chart of steps leading from MOUDI substrate collection to compilation of final data. The more commonly used single MOUDI sampling strategy follows only the top branch after “MOUDI” while the less frequent dual MOUDI sampling approach encompasses both the top and bottom branches. Rounded boxes represent instrument and analytical analyses steps while the standard boxes represent other processing steps.

Ion	Recovery \pm SD (%)	LOD (ppb)	LOQ (ppb)	LOD ($\mu\text{g m}^{-3}$)	LOQ ($\mu\text{g m}^{-3}$)
Adipate	101 \pm 4	22.655	75.517	2.10E-03	6.99E-03
Ammonium	100 \pm 17	42.434	141.447	3.93E-03	1.31E-02
Calcium	100 \pm 5	45.229	150.763	4.19E-03	1.40E-02
Chloride	103 \pm 7	2.144	7.147	1.99E-04	6.62E-04
DMA	100 \pm 2	52.709	175.697	4.88E-03	1.63E-02
Magnesium	104 \pm 8	36.925	123.083	3.42E-03	1.14E-02
Maleate	100 \pm 3	6.970	23.233	6.45E-04	2.15E-03
MSA	102 \pm 6	12.316	41.053	1.14E-03	3.80E-03
Nitrate	106 \pm 12	8.917	29.723	8.26E-04	2.75E-03
Oxalate	100 \pm 2	12.312	41.040	1.14E-03	3.80E-03
Phthalate	99 \pm 2	20.685	68.950	1.92E-03	6.38E-03
Pyruvate	102 \pm 6	63.754	212.513	5.90E-03	1.97E-02
Sodium	104 \pm 8	43.476	144.920	4.03E-03	1.34E-02
Succinate	98 \pm 9	11.046	36.820	1.02E-03	3.41E-03
Sulfate	101 \pm 3	11.982	39.940	1.11E-03	3.70E-03
TMA & DEA	102 \pm 4	315.164	1050.550	2.92E-02	9.73E-02

Table 4. Water-soluble species analyzed with their respective recoveries \pm standard deviations (SD), limits of detection (LOD), and limits of quantification (LOQ) in aqueous concentration units. Species were quantified using IC (ions). LODs and LOQs in ppb are aqueous concentrations while LODs and LOQs in $\mu\text{g m}^{-3}$ are air equivalent concentrations.

NO_3^- , and SO_4^{2-} using an eluent of potassium hydroxide (KOH). A 30-minute instrument method was used for both anion and cation columns with a 5-minute equilibration period giving a total of 35 minutes per sample. The columns used were the Dionex IonPac AS11-HC 250 mm and CS12A 250 mm models for anion and cation analysis, respectively. The suppressors used were a Dionex AERS 500e and a CERS 500e for anions and cations, respectively. For anions, the eluent started at 2 mM, ramped up to 8 mM from 0 to 20 minutes, and then ramped up from 8 to 28 mM from 20 to 30 minutes using a suppressor current of 28 mA. For cations, the eluent started at 5 mM, was isocratic from 0 to 13 minutes, ramped up from 5 to 18 mM from 13 to 16 minutes, and finally was isocratic at 18 mM from 16 to 30 minutes using a suppressor current of 22 mA. The recoveries, limits of detection (LOD), and limits of quantification (LOQ) for these species can be found in Table 4.

Elements. Water-soluble elements were speciated and quantified using ICP-QQQ after being acidified in 2% nitric acid. The elements quantified were: Ag, Al, As, Ba, Cd, Co, Cr, Cs, Cu, Fe, Hf, K, Mn, Mo, Nb, Ni, Pb, Rb, Se, Sn, Sr, Ti, Tl, V, Y, Zn, and Zr. The recoveries, LOD, and LOQ for these species can be found in Table 5. For species that were measured by both IC and ICP-QQQ (Na, Mg, K, and Ca), duplications were not included in the dataset. IC measurements are provided for Na, Mg, and Ca, while ICP-QQQ measurements for K are provided due to potential contamination from the eluent (i.e., KOH) used in the IC. The exception to this is for sets MO57-MO65 where K from the IC was used due to lack of ICP-QQQ data.

Gravimetric. Gravimetric analysis was performed using a Sartorius ME5-F microbalance with a sensitivity of $\pm 1 \mu\text{g}$. The microbalance was located in a temperature and humidity-controlled room at 20–23 °C and 30–40% relative humidity with an airlock buffer. Clean substrates were weighed prior to sample collection and then weighed again after sampling ended. Before weighing took place, the filters were equilibrated in the room for at least 24 hours. After the equilibration time, each substrate was passed near a ^{210}Po antistatic tip for 30 seconds to minimize measurement bias due to electrostatic charge at the surface of the substrate. Each substrate was weighed twice, once initially and then again 24 hours later. If the difference between these two weighings exceeded $10 \mu\text{g}$, the substrate was weighed again 24 hours later and this process was repeated until the difference between weighings was less than $10 \mu\text{g}$. The percent standard deviations for the weighings before and after sampling, respectively, were relatively negligible, with the highest being 0.005%. The PM mass was derived from the difference of the average substrate weight after sampling minus the average substrate weight before sampling. The standard deviation of the change in weight was then calculated for each PM substrate using the following error propagation equation:

$$SD_d = \sqrt{SD_b^2 + SD_a^2} \quad (1)$$

where SD_d is the standard deviation of the difference, SD_b is the standard deviation of the substrate before sampling, and SD_a is the standard deviation of the substrate after sampling. The percent standard deviation across all stages and sets averaged out to be approximately 7%.

Black carbon. The subsequently weighed substrates were then analyzed using a Multi-wavelength Absorption Black Carbon Instrument (MABI; Australian Nuclear Science and Technology Organisation). The MABI is an optical instrument used to quantify the mass concentration of black carbon by detecting the absorption for seven

Element	Recovery \pm SD (%)	LOD (ppt)	LOQ (ppt)	LOD ($\mu\text{g m}^{-3}$)	LOQ ($\mu\text{g m}^{-3}$)
Ag	100 \pm 11	0.743	2.477	6.88E-08	2.29E-07
Al	96 \pm 7	29.474	98.247	2.73E-06	9.10E-06
As	98 \pm 10	7.945	26.483	7.36E-07	2.45E-06
Ba	97 \pm 11	3.698	12.327	3.42E-07	1.14E-06
Cd	102 \pm 11	4.194	13.980	3.88E-07	1.29E-06
Co	98 \pm 8	0.722	2.407	6.69E-08	2.23E-07
Cr	97 \pm 9	1.150	3.833	1.06E-07	3.55E-07
Cs	—	0.733	2.443	6.79E-08	2.26E-07
Cu	99 \pm 8	1.127	3.757	1.04E-07	3.48E-07
Fe	97 \pm 9	1.191	3.970	1.10E-07	3.68E-07
Hf	—	0.963	3.210	8.92E-08	2.97E-07
K	93 \pm 18	10.480	34.933	9.70E-07	3.23E-06
Mn	97 \pm 9	1.624	5.413	1.50E-07	5.01E-07
Mo	96 \pm 11	2.258	7.527	2.09E-07	6.97E-07
Nb	—	0.522	1.740	4.83E-08	1.61E-07
Ni	97 \pm 8	2.837	9.457	2.63E-07	8.76E-07
Pb	99 \pm 8	0.503	1.677	4.66E-08	1.55E-07
Rb	—	1.566	5.220	1.45E-07	4.83E-07
Se	97 \pm 10	82.393	274.643	7.63E-06	2.54E-05
Sn	97 \pm 7	1.772	5.907	1.64E-07	5.47E-07
Sr	98 \pm 9	1.102	3.673	1.02E-07	3.40E-07
Ti	101 \pm 10	39.046	130.153	3.62E-06	1.21E-05
Tl	100 \pm 8	0.383	1.277	3.55E-08	1.18E-07
V	95 \pm 9	1.353	4.510	1.25E-07	4.18E-07
Y	—	0.523	1.743	4.84E-08	1.61E-07
Zn	96 \pm 8	5.880	19.600	5.44E-07	1.81E-06
Zr	—	1.008	3.360	9.33E-08	3.11E-07

Table 5. Same as Table 4 but species were quantified using ICP-QQQ (elements). Species marked with ‘—’ in their respective recovery and standard deviation columns were not measured for recovery purposes. LODs and LOQs in ppt are aqueous concentrations while LODs and LOQs in $\mu\text{g m}^{-3}$ are air equivalent concentrations.

wavelengths (405, 465, 525, 639, 870, 940, and 1050 nm). The following equation was used to calculate black carbon concentration:

$$BC(\text{ng m}^{-3}) = \frac{10^5[A(\text{cm}^2)]}{[\epsilon(\text{m}^2 \text{g}^{-1})][V(\text{m}^3)]} \ln\left[\frac{I_0}{I}\right] \quad (2)$$

where ϵ is the mass absorption coefficient, A is the substrate collection area, V is the volume of air sampled, I_0 is the measured light transmission through the blank substrate, and I is the measured light transmitted through the sample substrate. The mass absorption coefficient was provided in the MABI manual, collection area was retrieved based on impaction rings on the substrates, volume was calculated from flowrate and sample time, and light transmission was produced directly from the MABI.

Data processing. IC and ICP-QQQ areas were converted to concentrations using Excel sheets formatted to use calibration curves, unit operations, and sampling information. The concentration files were then organized using an assortment of MATLAB codes to produce the data into the published state with gravimetric and black carbon data. Excel and MATLAB processing files are available upon request.

Data Records

The dataset, located on figshare⁴⁰, is in a specialized format used by the National Aeronautics and Space Administration (NASA) for field data, which is referred to as the ICARTT file format. The file name consists of the associated campaign, instrument used, sampling method, start date, revision number, and the end date. The format includes data notes in a README tab. These notes include the data principal investigator (PI), affiliated institution, mission name, the start date of data collection, the last data revision date, the number of variables, data flags, sampling platform and location, instrument information, brief description of the data, and revision log. The revision log states what revision the data is currently on and lists the previous revisions and their relative status. Additional tabs include the MOUDI stage cutpoints and size ranges, uncertainties and LODs, and the variable list and units. Data include ions, elements, gravimetric weights, and MABI measurements separated by stages in air equivalent mass concentrations ($\mu\text{g m}^{-3}$). Note that the reported data are in air equivalent concentrations and typically are converted to $dC/d\log D_p$ to properly look at the size distributions.

Technical Validation

A number of experimental and data processing techniques were implemented to validate and better characterize the final data. The flowrate for each set was measured using a flowmeter (Mesa Labs Definer 220 series) three times both prior to and after each sampling period. The overall average of these values was used as the flowrate for each set. Additionally, pressures for each stage were measured at the beginning and end of sampling to ensure there was no significant change in the pressure drop. To keep the flowrate as close to 30 L min⁻¹ as possible, the MOUDI nozzle plates were removed and cleaned regularly and especially if the flowrate dropped below 27 L min⁻¹. The nozzle plates were cleaned by soaking the plates in either a methanol-water solution or in pure methanol for 24 hours or more. They were then removed and rinsed with methanol, followed by placement in a clean area to let the methanol evaporate. However, towards the ending of the sampling campaign the flowrate dropped to about 24 L min⁻¹ and subsequent cleanings did not alleviate the problem. The issue was likely due to one or both of the lower nozzle plates (0.056 and 0.1 μm cutpoint diameters) being heavily clogged with the black carbon rich air and unable to be cleared without a more aggressive cleaning method.

Chromatogram peaks were automatically drawn by the IC and ICP-QQQ system software. However, for the IC only, the operator would view each chromatogram to adjust peak areas and add in missing species. LOD and LOQ were calculated using 3 S_bb⁻¹ and 10 S_bb⁻¹ methods, respectively, where S_b is the standard deviation of the response and b is the slope of the calibration curve⁴¹. Recoveries were calculated by taking the ratio of the mass of a specific measured species to the known amount of that species in that sample⁴². Recoveries for IC and ICP-QQQ were all above 93% with repeatability ranging from 2% to 18% (Tables 4 and 5). During data analysis, dC/dlog D_p plots (stages 2–11) were examined to ensure a normal distribution was obtained. If the first (stage 2) or last stage (stage 11) was higher than the next (stage 3) or previous stage (stage 10), respectively, then that stage was not considered for a particular set and viewed as having unreliable data. If a species was not measured for a stage, a value of -9999 was inputted. Similarly, if a species was below the LOD for a stage, a value of -8888 was inputted. A summary of the relative number of data points either missing (i.e., no ICP-QQQ data for last seven sets) or below the LOD for a specific species and stage can be seen in Table 6.

A charge balance was also performed by converting each species to moles, multiplying by their respective charges, and then summing up all cations and all anions in a stage. It should be noted that only IC species, with the exception of K from ICP-QQQ, were used to measure the overall charge balances. The reasons for these are (i) the majority of the ICP-QQQ species are transition metals which have varying oxidation states and, without pH measurements, the proper charge cannot be assigned, and (ii) the majority of these species are very low in concentration and do not significantly affect the overall charge balances. All the stages were then plotted per set and a trend line was applied to test if there was a linear correlation. The charge balance R² values in Table 7 reveal strong linear correlations (> 0.90), verifying that the data are valid. Additionally, Fig. 3 shows the overall charge balance for every set. All of the sets agree with the trend, with the exception of set 24, which can be seen deviating from the rest of the data. This set coincided with New Year's fireworks, which produce a large amount of anionic species such as sulfate and nitrate as well as cationic metals, such as Fe and Cu. The combination of large anionic concentrations and the presence of cationic metals not included in the calculation lead to a charge balance slope below unity (i.e. more anions than cations).

Usage Notes

The data provided can be used to conduct various studies to improve understanding of regional PM effects and implications. The dataset can be synchronized up with the other CHECSM instruments set up by the Air Quality Dynamics-Instrumentation and Technology Development (AQD-ITD) laboratory, the AEROSOL ROBOTIC NETWORK (AERONET) station⁴³, and meteorological and precipitation chemistry data collected by MO (Table 2).

There are a host of previous (7 SouthEast Asian Studies (7-SEAS) 2010–2018; Biomass-burning Aerosols & Stratocumulus Environment: Lifecycles and Interactions Experiment (BASELInE) 2013–2015) and ongoing (CAMP²Ex) research activities in southeast Asia from which this dataset can provide additional context. The dataset also has relevance for all global regions in that process-level understanding can be improved using a dataset with such a wide range of pollution scenarios in one of the most polluted cities of the world with diverse meteorological characteristics.

A few papers have been produced using portions of this dataset already. Cruz *et al.*¹⁶ looked at size-resolved PM composition during the 2018 southwest monsoon season and conducted positive matrix factorization (PMF) to identify PM sources, which were attributed to aged PM, sea salt, combustion emissions, vehicular/resuspended dust, and waste processing emissions. Braun *et al.*¹⁸ presented case examples of long-range transport of PM from east and southeast Asia, such as biomass burning from the Maritime Continent and transport from continental East Asia. They also presented examples of different transport pathways of pollution to the study site which yielded concentration differences for species such as K, Rb, Ba, V, Pb, Mo, and Sn. AzadiAghdam *et al.*¹⁷ analyzed sea salt PM in Metro Manila and found that sea salt concentrations varied during the wet season and appeared to be contaminated by crustal and anthropogenic sources. Building off these limited examples using just a subset of the overall dataset, there are a significant number of topics that this dataset can be used to address, such as the following:

- Impacts of PM on regional climate, clouds, and monsoon activity by (i) comparing PM composition to other cities around the world with and without monsoon seasons, (ii) combining the dataset with meteorological data from satellites and models to understand influences on aerosol composition via mechanisms such as photochemical processing, and (iii) relating surface PM concentrations to AOD from AERONET and satellite sensors to examine the vertical nature of aerosol in the region as has been done in other regions (e.g. ref. ⁴⁴).

Species	Stage 1	Stage 2	Stage 3	Stage 4	Stage 5	Stage 6	Stage 7	Stage 8	Stage 9	Stage 10	Stage 11	Stage 12
Ag	7(39)	7(42)	7(31)	7(32)	7(30)	7(30)	7(30)	7(29)	7(27)	7(33)	7(40)	7(40)
Al	7(5)	7(5)	7(0)	7(0)	7(0)	7(0)	7(0)	7(0)	7(1)	7(1)	7(23)	7(19)
As	7(41)	7(44)	7(39)	7(35)	7(34)	7(21)	7(4)	7(5)	7(5)	7(8)	7(37)	7(40)
Ba	7(5)	7(0)	7(0)	7(0)	7(0)	7(0)	7(0)	7(0)	7(0)	7(16)	7(33)	7(26)
Cd	7(36)	7(41)	7(35)	7(30)	7(27)	7(6)	7(0)	7(0)	7(0)	7(8)	7(33)	7(37)
Co	7(24)	7(31)	7(18)	7(11)	7(7)	7(11)	7(12)	7(12)	7(11)	7(25)	7(40)	7(35)
Cr	7(27)	7(27)	7(14)	7(14)	7(14)	7(14)	7(6)	7(12)	7(14)	7(14)	7(16)	7(14)
Cs	7(47)	7(46)	7(37)	7(23)	7(23)	7(11)	7(3)	7(0)	7(0)	7(2)	7(41)	7(46)
Cu	7(28)	7(28)	7(8)	7(8)	7(7)	7(7)	7(3)	7(2)	7(7)	7(8)	7(14)	7(13)
Fe	7(18)	7(21)	7(12)	7(4)	7(2)	7(4)	7(1)	7(2)	7(10)	7(16)	7(25)	7(17)
Hf	7(45)	7(47)	7(41)	7(34)	7(31)	7(40)	7(37)	7(41)	7(44)	7(42)	7(47)	7(47)
K	0(14)	0(12)	0(1)	0(0)	0(0)	0(0)	0(0)	0(0)	0(0)	0(0)	0(15)	0(15)
Mn	7(3)	7(1)	7(0)	7(0)	7(0)	7(0)	7(0)	7(0)	7(0)	7(0)	7(15)	7(15)
Mo	7(37)	7(40)	7(23)	7(12)	7(8)	7(6)	7(4)	7(4)	7(4)	7(8)	7(34)	7(38)
Nb	7(43)	7(44)	7(35)	7(28)	7(23)	7(30)	7(17)	7(25)	7(34)	7(44)	7(47)	7(41)
Ni	7(26)	7(26)	7(3)	7(3)	7(1)	7(1)	7(0)	7(0)	7(0)	7(2)	7(10)	7(17)
Pb	7(25)	7(24)	7(3)	7(0)	7(0)	7(0)	7(0)	7(0)	7(0)	7(0)	7(13)	7(13)
Rb	7(10)	7(8)	7(2)	7(0)	7(0)	7(0)	7(0)	7(0)	7(0)	7(0)	7(8)	7(12)
Se	7(37)	7(43)	7(27)	7(25)	7(14)	7(13)	7(11)	7(11)	7(16)	7(24)	7(39)	7(39)
Sn	7(38)	7(40)	7(35)	7(22)	7(18)	7(8)	7(4)	7(0)	7(1)	7(5)	7(36)	7(36)
Sr	7(1)	7(1)	7(0)	7(0)	7(0)	7(0)	7(0)	7(0)	7(7)	7(14)	7(23)	7(18)
Ti	7(12)	7(8)	7(0)	7(0)	7(0)	7(0)	7(2)	7(3)	7(2)	7(6)	7(24)	7(21)
Tl	15(35)	15(36)	15(34)	15(35)	15(34)	15(31)	15(20)	15(18)	15(21)	15(27)	15(34)	15(34)
V	7(41)	7(41)	7(33)	7(26)	7(23)	7(16)	7(4)	7(0)	7(1)	7(18)	7(40)	7(40)
Y	7(33)	7(35)	7(22)	7(15)	7(14)	7(22)	7(26)	7(32)	7(29)	7(33)	7(39)	7(40)
Zn	7(11)	7(13)	7(5)	7(0)	7(0)	7(0)	7(0)	7(0)	7(0)	7(0)	7(12)	7(12)
Zr	7(31)	7(36)	7(14)	7(5)	7(1)	7(7)	7(9)	7(21)	7(36)	7(30)	7(42)	7(34)
Adipate	4(39)	4(42)	4(22)	4(30)	4(30)	4(30)	4(32)	4(29)	4(25)	4(20)	4(39)	4(37)
Ammonium	0(28)	0(37)	0(11)	0(8)	0(6)	0(2)	0(1)	0(0)	0(0)	0(0)	0(10)	0(8)
Calcium	0(15)	0(14)	0(2)	0(0)	0(0)	0(0)	0(1)	0(5)	0(8)	0(15)	0(41)	0(33)
Chloride	0(11)	0(8)	0(1)	0(0)	0(0)	0(0)	0(0)	0(2)	0(2)	0(7)	0(39)	0(30)
DMA	0(52)	0(53)	0(43)	0(47)	0(47)	0(39)	0(27)	0(25)	0(29)	0(41)	0(46)	0(44)
Magnesium	0(12)	0(9)	0(0)	0(0)	0(0)	0(0)	0(0)	0(1)	0(1)	0(12)	0(34)	0(34)
Maleate	0(54)	0(54)	0(53)	0(49)	0(51)	0(48)	0(24)	0(16)	0(23)	0(52)	0(54)	0(53)
MSA	0(49)	0(51)	0(44)	0(42)	0(28)	0(22)	0(7)	0(4)	0(8)	0(11)	0(48)	0(49)
Nitrate	0(20)	0(19)	0(2)	0(0)	0(0)	0(0)	0(1)	0(1)	0(1)	0(5)	0(31)	0(21)
Oxalate	0(14)	0(13)	0(5)	0(0)	0(0)	0(0)	0(0)	0(0)	0(0)	0(0)	0(6)	0(20)
Phthalate	0(47)	0(51)	0(38)	0(19)	0(20)	0(31)	0(24)	0(24)	0(23)	0(42)	0(51)	0(44)
Pyruvate	0(48)	0(53)	0(50)	0(50)	0(48)	0(51)	0(51)	0(54)	0(53)	0(52)	0(54)	0(51)
Sodium	0(13)	0(12)	0(1)	0(0)	0(0)	0(0)	0(0)	0(0)	0(0)	0(1)	0(24)	0(19)
Succinate	0(48)	0(50)	0(43)	0(41)	0(38)	0(42)	0(35)	0(35)	0(41)	0(47)	0(52)	0(47)
Sulfate	0(11)	0(8)	0(0)	0(0)	0(0)	0(0)	0(0)	0(0)	0(0)	0(0)	0(1)	0(9)
TMA & DEA	0(54)	0(54)	0(54)	0(54)	0(54)	0(52)	0(39)	0(32)	0(34)	0(46)	0(53)	0(54)

Table 6. Summary of the number of data points either missing (outside parenthesis) or below the LOD (inside parenthesis) for a given species and MOUDI stage. Note that there were a total of 54 possible data points for each species and stage. These counts exclude gravimetric and microscopy sets where chemical analysis was not performed. Refer to Table 3 for cutpoint diameters and diameter ranges.

- Removal of PM via wet deposition by looking at what species are most effectively scavenged using precipitation data (e.g. refs. ^{45,46}).
- Aqueous processing of PM by looking at the changes of PM concentrations in the dry vs the wet season and additionally as a function of cloud coverage and aerosol liquid water amounts (e.g. refs. ^{47,48}).
- Source apportionment of PM by (i) observing seasonal changes in emissions (e.g. ref. ⁴⁹) and (ii) comparing the emission sources determined by techniques such as PMF for the 2018 southwest monsoon season versus the 2019 southwest monsoon season.
- Effects associated with mixing of varying air masses (e.g. ref. ⁵⁰) by identifying (i) what air masses influence the city and during what times of year, (ii) if synergistic effects of mixing air masses can be seen year round, and (iii) if satellites and models that speciate aerosol can capture the behavior of mixing air masses in the region as reflected in the MOUDI data.

Set #	Slope	R ²	Set #	Slope	R ²
MO1	0.89	0.92	MO31/32	1.19	0.94
MO2	1.42	0.99	MO33	1.26	0.95
MO3/4	1.21	1.00	MO34	1.43	0.98
MO5	1.36	0.99	MO35/36	1.36	1.00
MO6	1.32	0.98	MO37	1.37	0.94
MO7	1.36	0.99	MO38	1.29	0.95
MO8	1.36	1.00	MO39/40	1.50	0.97
MO9	1.26	0.99	MO41	1.50	0.99
MO10	1.35	1.00	MO42	1.46	0.96
MO11	1.26	0.84	MO43/44	1.44	1.00
MO12	1.33	0.99	MO45	1.35	1.00
MO13/14	1.29	1.00	MO46	1.47	1.00
MO15	1.30	0.99	MO47	1.60	0.99
MO16	1.42	0.98	MO48/49	1.70	0.97
MO17	1.39	0.96	MO50	1.94	0.99
MO18	1.33	0.98	MO51	1.43	0.94
MO19	1.47	0.98	MO52/53	1.63	0.94
MO20	1.29	0.95	MO54	1.46	1.00
MO21	1.30	0.97	MO55	1.38	0.98
MO22	1.27	0.97	MO56	1.57	0.94
MO23	1.27	0.94	MO57/58	1.24	0.96
MO24	0.82	1.00	MO59	1.45	1.00
MO26	1.46	0.91	MO60	1.29	0.96
MO27	1.55	1.00	MO61	1.39	0.97
MO28	1.17	0.97	MO62/63	1.24	0.97
MO29	1.50	0.87	MO64	1.36	1.00
MO30	1.66	0.91	MO65/66	1.44	0.99

Table 7. Slope and coefficient of determination (R²) of the water-soluble charge balance for each MOUDI set. Values above 1 indicate there is an anion deficit. Only IC species and K from ICP-QQQ are taken into consideration for the charge balance calculations.

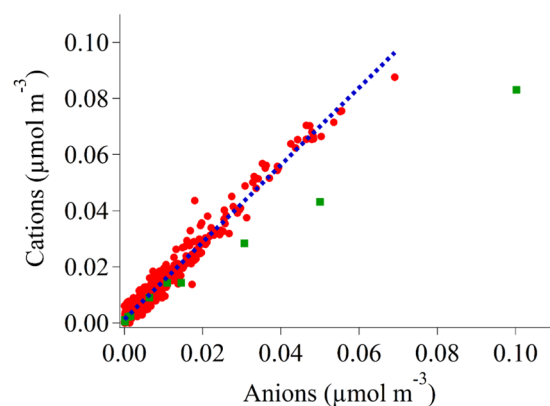


Fig. 3 Charge balance plot for the cumulative MOUDI dataset using individual stages of all MOUDI sets. Red dots represent every stage of every set, with the exclusion of set 24, which is represented as green squares. The blue dashed line represents the line of best fit with a slope of 1.38 ± 0.01 and a R² value of 0.97, excluding set 24, which was associated with New Year's fireworks containing elevated anions and cationic transition metals.

- Catalytic and destructive effects of metals on inorganic (e.g. refs. ^{51–53}) and organic species (e.g. refs. ^{54–56}).
- Impacts of extreme events on regional PM by examining (i) sets where holidays occurred (e.g. New Year's) and (ii) sets influenced by typhoons, which have been shown to impact aerosol in the general region, such as was shown in previous studies in Taiwan⁵⁷.
- Public health implications related to PM by examining the characteristic size distributions of species posing negative effects such as heavy metals and their general prevalence in Metro Manila.

Received: 19 February 2020; Accepted: 30 March 2020;

Published online: 29 April 2020

References

- Pope, C. A. & Dockery, D. W. Health effects of fine particulate air pollution: lines that connect. *J. Air Waste Manag. Assoc.* **56**, 709–742 (2006).
- IPCC. Climate Change 2013: The Physical Science Basis. (2013).
- Ramanathan, V., Crutzen, P. J., Kiehl, J. T. & Rosenfeld, D. Aerosols, climate, and the hydrological cycle. *Science* **294**, 2119–2124 (2001).
- Brunner, U. & Bachofen, R. The biogeochemical cycles of phosphorus: a review of local and global consequences of the atmospheric input. *Toxicol. Environ. Chem.* **67**, 171–188 (1998).
- Rajput, P., Izhar, S. & Gupta, T. Deposition modeling of ambient aerosols in human respiratory system: health implication of fine particles penetration into pulmonary region. *Atmos. Pollut. Res* **10**, 334–343 (2019).
- Anselm, A., Heibel, T., Gebhart, J. & Ferron, G. *In vivo*-studies of growth factors of sodium chloride particles in the human respiratory tract. *J. Aerosol Sci.* **21**, S427–S430 (1990).
- Byron, P. R., Davis, S. S., Bubb, M. D. & Cooper, P. Pharmaceutical implications of particle growth at high relative humidities. *Pestic. Sci.* **8**, 521–526 (1977).
- Shingler, T. *et al.* Ambient observations of hygroscopic growth factor and $f(RH)$ below 1: case studies from surface and airborne measurements. *J. Geophys. Res.-Atmos* **121**(13), 661–613,677 (2016).
- Barbaro, E. *et al.* Characterization of the water soluble fraction in ultrafine, fine, and coarse atmospheric aerosol. *Sci. Total Environ.* **658**, 1423–1439 (2019).
- Braun, R. A. *et al.* Impact of wildfire emissions on chloride and bromide depletion in marine aerosol particles. *Environ. Sci. Technol.* **51**, 9013–9021 (2017).
- Alas, H. D. *et al.* Spatial characterization of black carbon mass concentration in the atmosphere of a southeast asian megacity: an air quality case study for Metro Manila, Philippines. *Aerosol Air Qual. Res* **18**, 2301–2317 (2018).
- PSA. *Highlights of the Philippine population 2015 census of population*, <https://psa.gov.ph/content/highlights-philippine-population-2015-census-population> (2016).
- Kim Oanh, N. T. *et al.* Particulate air pollution in six asian cities: spatial and temporal distributions, and associated sources. *Atmos. Environ.* **40**, 3367–3380 (2006).
- Bautista, A. T., Pabroa, P. C. B., Santos, F. L., Racho, J. M. D. & Quirin, L. L. Carbonaceous particulate matter characterization in an urban and a rural site in the Philippines. *Atmos. Pollut. Res* **5**, 245–252 (2014).
- Kecorius, S. *et al.* Aerosol particle mixing state, refractory particle number size distributions and emission factors in a polluted urban environment: case study of Metro Manila, Philippines. *Atmos. Environ.* **170**, 169–183 (2017).
- Cruz, M. T. *et al.* Size-resolved composition and morphology of particulate matter during the southwest monsoon in Metro Manila, Philippines. *Atmos. Chem. Phys.* **19**, 10675–10696 (2019).
- AzadiAghdam, M. *et al.* On the nature of sea salt aerosol at a coastal megacity: insights from Manila, Philippines in southeast asia. *Atmos. Environ.* **216**, 116922 (2019).
- Braun, R. A. *et al.* Long-range aerosol transport and impacts on size-resolved aerosol composition in Metro Manila, Philippines. *Atmos. Chem. Phys.* **20**, 2387–2405, <https://doi.org/10.5194/acp-20-2387-2020> (2020).
- PAGASA. *Onset of the rainy season*, <http://bagong.pagasa.dost.gov.ph/press-release/29#> (2018).
- PAGASA. *Termination of the southwest monsoon*, <http://bagong.pagasa.dost.gov.ph/press-release/30> (2018).
- PAGASA. *Onset of the northeast monsoon*, <http://bagong.pagasa.dost.gov.ph/press-release/32> (2018).
- Rappler. *Southwest monsoon begins, but not yet rainy season*, <https://amp.rappler.com/nation/special-coverage/weather-alert/232803-pagasa-forecast-southwest-monsoon-begins-2019>.
- Inquirer. *From habagat to amihan: colder days ahead in PH*, <https://newsinfo.inquirer.net/1174623/from-habagat-to-amihan-colder-days-ahead-in-ph> (2019).
- Marple, V. *et al.* Second generation micro-orifice uniform deposit impactor, 120 MOUDI-II: design, evaluation, and application to long-term ambient sampling. *Aerosol Sci. Tech.* **48**, 427–433 (2014).
- Fonseca, A. S. *et al.* Intercomparison of four different cascade impactors for fine and ultrafine particle sampling in two european locations. *Atmos. Chem. Phys. Discuss.* (2016).
- Laskin, A., Iedema, M. J. & Cowin, J. P. Quantitative time-resolved monitoring of nitrate formation in sea salt particles using a CCSEM/EDX single particle analysis. *Environ. Sci. Technol.* **36**, 4948–4955 (2002).
- Laskin, A. *et al.* Tropospheric chemistry of internally mixed sea salt and organic particles: surprising reactivity of NaCl with weak organic acids. *J. Geophys. Res.-Atmos.* **117**, D15302 (2012).
- Hamacher-Barth, E., Jansson, K. & Leck, C. A method for sizing submicrometer particles in air collected on formvar films and imaged by scanning electron microscope. *Atmos. Meas. Tech* **6**, 3459–3475 (2013).
- Asa-Awuku, A., Sullivan, A., Hennigan, C., Weber, R. & Nenes, A. Investigation of molar volume and surfactant characteristics of water-soluble organic compounds in biomass burning aerosol. *Atmos. Chem. Phys.* **8**, 799–812 (2008).
- Baumann, K., Ift, F., Zhao, J. Z. & Chameides, W. L. Discrete measurements of reactive gases and fine particle mass and composition during the 1999 Atlanta Supersite Experiment. *J. Geophys. Res.-Atmo* **108**, 8416 (2003).
- Sullivan, A. P. & Weber, R. J. Chemical characterization of the ambient organic aerosol soluble in water: 2. Isolation of acid, neutral, and basic fractions by modified size-exclusion chromatography. *J. Geophys. Res.-Atmo.* **111**, D05315 (2006).
- Bozzetti, C. *et al.* Organic aerosol source apportionment by offline-AMS over a full year in Marseille. *Atmos. Chem. Phys.* **17**, 8247–8268 (2017).
- Behera, S. N., Cheng, J. & Balasubramanian, R. *In situ* acidity and pH of size-fractionated aerosols during a recent smoke-haze episode in Southeast Asia. *Environ. Geochem. Health* **37**, 843–859 (2015).
- Fang, T., Guo, H., Verma, V., Peltier, R. E. & Weber, R. J. PM 2.5 water-soluble elements in the southeastern United States: automated analytical method development, spatiotemporal distributions, source apportionment, and implications for health studies. *Atmos. Chem. Phys.* **15**, 11667–11682 (2015).
- Heal, M. R., Hibbs, L. R., Agius, R. M. & Beverland, I. J. Total and water-soluble trace metal content of urban background PM 10, PM 2.5 and black smoke in Edinburgh, UK. *Atmos. Environ.* **39**, 1417–1430 (2005).
- Jiang, S. Y. N., Yang, F., Chan, K. L. & Ning, Z. Water solubility of metals in coarse PM and PM 2.5 in typical urban environment in Hong Kong. *Atmos. Pollut. Res* **5**, 236–244 (2014).
- Knaapen, A. M., Shi, T., Borm, P. J. A. & Schins, R. P. F. Soluble metals as well as the insoluble particle fraction are involved in cellular DNA damage induced by particulate matter. *Mol. Cell. Biochem* **234/235**, 317–326 (2002).
- Lindberg, S. E. & Harriss, R. C. Water and acid soluble trace metals in atmospheric particles. *J. Geophys. Res.-Oceans* **88**, 5091–5100 (1983).
- Sarti, E. *et al.* The composition of PM 1 and PM 2.5 samples, metals and their water soluble fractions in the Bologna area (Italy). *Atmos. Pollut. Res* **6**, 708–718 (2015).

40. Stahl, C. *et al.* An annual time series of weekly size-resolved aerosol properties in the megacity of Metro Manila, Philippines. *Figshare* <https://doi.org/10.6084/m9.figshare.11861859.v2> (2020).
41. Shrivastava, A. & Gupta, V. Methods for the determination of limit of detection and limit of quantitation of the analytical methods. *Chron. Young Sci* **2**, 21–25 (2011).
42. Perrino, C. *et al.* Improved time-resolved measurements of inorganic ions in particulate matter by PILS-IC integrated with a sample pre-concentration system. *Aerosol Sci. Tech.* **49**, 521–530 (2015).
43. Holben, B. N. *et al.* AERONET—a federated instrument network and data archive for aerosol characterization. *Remote Sens. Environ.* **66**, 1–16 (1998).
44. van Donkelaar, A., Martin, R. V. & Park, R. J. Estimating ground-level PM 2.5 using aerosol optical depth determined from satellite remote sensing. *J. Geophys. Res.-Atmos.* **111**, D21201 (2006).
45. Wu, Y. *et al.* Comparison of dry and wet deposition of particulate matter in near-surface waters during summer. *Plos One* **13**, e0199241 (2018).
46. MacDonald, A. B. *et al.* Characteristic vertical profiles of cloud water composition in marine stratocumulus clouds and relationships with precipitation. *J. Geophys. Res. Atmos* **123**, 3704–3723 (2018).
47. McNeill, V. F. Aqueous organic chemistry in the atmosphere: sources and chemical processing of organic aerosols. *Environ. Sci. Technol.* **49**, 1237–1244 (2015).
48. Ervens, B. *et al.* Is there an aerosol signature of chemical cloud processing? *Atmos. Chem. Phys.* **18**, 16099–16119 (2018).
49. Kumar, R. *et al.* What controls the seasonal cycle of black carbon aerosols in India? *J. Geophys. Res.-Atmos* **120**, 7788–7812 (2015).
50. Weber, R. J. *et al.* A study of secondary organic aerosol formation in the anthropogenic-influenced southeastern United States. *J. Geophys. Res.-Atmos.* **112**, D13302 (2007).
51. Sorooshian, A. *et al.* Surface and airborne measurements of organosulfur and methanesulfonate over the western United States and coastal areas. *J. Geophys. Res.-Atmos* **120**, 8535–8548 (2015).
52. Gaston, C. J., Pratt, K. A., Qin, X. & Prather, K. A. Real-time detection and mixing state of methanesulfonate in single particles at an inland urban location during a phytoplankton bloom. *Environ. Sci. Technol.* **44**, 1566–1572 (2010).
53. Ault, A. P. *et al.* Characterization of the single particle mixing state of individual ship plume events measured at the port of Los Angeles. *Environ. Sci. Technol.* **44**, 1954–1961 (2010).
54. Furukawa, T. & Takahashi, Y. Oxalate metal complexes in aerosol particles: implications for the hygroscopicity of oxalate-containing particles. *Atmos. Chem. Phys.* **11**, 4289–4301 (2011).
55. Crahan, K. K., Hegg, D., Covert, D. S. & Jonsson, H. An exploration of aqueous oxalic acid production in the coastal marine atmosphere. *Atmos. Environ.* **38**, 3757–3764 (2004).
56. Sorooshian, A., Wang, Z., Coggon, M. M., Jonsson, H. H. & Ervens, B. Observations of sharp oxalate reductions in stratocumulus clouds at variable altitudes: organic acid and metal measurements during the 2011 E-PEACE campaign. *Environ. Sci. Technol.* **47**, 7747–7756 (2013).
57. Khan, M., Yin, Y., Anjum, A. & Yong, W. Impact assessment of cloud condensation nuclei (CCN) concentration on a typhoon evolution; a numerical case study. *Pakistan J. Meteo* **14**, 49–63 (2017).
58. Becagli, S. *et al.* Study of present-day sources and transport processes affecting oxidised sulphur compounds in atmospheric aerosols at dome c (Antarctica) from year-round sampling campaigns. *Atmos. Environ.* **52**, 98–108 (2012).
59. Thongsanit, P., Jinsart, W., Hooper, B., Hooper, M. & Limpaseni, W. Atmospheric particulate matter and polycyclic aromatic hydrocarbons for PM 10 and size-segregated samples in Bangkok. *J. Air Waste Manag. Assoc* **53**, 1490–1498 (2003).
60. Tan, J.-H. *et al.* Chemical characteristics of haze during summer and winter in Guangzhou. *Atmos. Res.* **94**, 238–245 (2009).
61. Wang, X. *et al.* The secondary formation of inorganic aerosols in the droplet mode through heterogeneous aqueous reactions under haze conditions. *Atmos. Environ.* **63**, 68–76 (2012).
62. Tsai, J. H., Chang, L. P. & Chiang, H. L. Size mass distribution of water-soluble ionic species and gas conversion to sulfate and nitrate in particulate matter in southern Taiwan. *Environ. Sci. Pollut. Res. Int* **20**, 4587–4602 (2013).
63. Li, X. *et al.* Characterization of the size-segregated water-soluble inorganic ions in the Jing-Jin-Ji urban agglomeration: spatial/temporal variability, size distribution and sources. *Atmos. Environ.* **77**, 250–259 (2013).
64. Zhu, Y. *et al.* Airborne particulate polycyclic aromatic hydrocarbon (PAH) pollution in a background site in the north China plain: concentration, size distribution, toxicity and sources. *Sci. Total Environ.* **466–467**, 357–368 (2014).
65. Verma, M. K., Singh Chauhan, L. K., Sultana, S. & Kumar, S. The traffic linked urban ambient air superfine and ultrafine PM 1 mass concentration, contents of pro-oxidant chemicals, and their seasonal drifts in Lucknow, India. *Atmos. Pollut. Res* **5**, 677–685 (2014).
66. Tsai, J. H., Chang, L. P. & Chiang, H. L. Airborne pollutant characteristics in an urban, industrial and agricultural complex metroplex with high emission loading and ammonia concentration. *Sci. Total Environ.* **494–495**, 74–83 (2014).
67. Sun, K. *et al.* Chemical characterization of size-resolved aerosols in four seasons and hazy days in the megacity Beijing of China. *J. Environ. Sci.-China* **32**, 155–167 (2015).
68. Chen, H.-W., Chen, W.-Y., Chang, C.-N., Chuang, Y.-H. & Lin, Y.-H. Identifying airborne metal particles sources near an optoelectronic and semiconductor industrial park. *Atmos. Res.* **174–175**, 97–105 (2016).
69. Gao, Y., Lee, S.-C., Huang, Y., Chow, J. C. & Watson, J. G. Chemical characterization and source apportionment of size-resolved particles in Hong Kong sub-urban area. *Atmos. Res.* **170**, 112–122 (2016).
70. Wan, X. *et al.* Chemical composition of size-segregated aerosols in Lhasa city, Tibetan Plateau. *Atmos. Res.* **174–175**, 142–150 (2016).
71. Yu, P. *et al.* Characteristics of dimethylammonium and trimethylammonium in atmospheric particles ranging from supermicron to nanometer sizes over eutrophic marginal seas of China and oligotrophic open oceans. *Sci. Total Environ.* **572**, 813–824 (2016).
72. Liu, Z. *et al.* Size-resolved aerosol water-soluble ions during the summer and winter seasons in Beijing: formation mechanisms of secondary inorganic aerosols. *Chemosphere* **183**, 119–131 (2017).
73. Begam, G. R. *et al.* Seasonal characteristics of water-soluble inorganic ions and carbonaceous aerosols in total suspended particulate matter at a rural semi-arid site, Kadapa (India). *Environ. Sci. Pollut. Res. Int* **24**, 1719–1734 (2017).
74. Ding, X. X. *et al.* Characteristics of size-resolved atmospheric inorganic and carbonaceous aerosols in urban Shanghai. *Atmos. Environ.* **167**, 625–641 (2017).
75. Li, Y. *et al.* Pollution characteristics of water-soluble ions in aerosols in the urban area in Beibei of Chongqing. *Aerosol Air Qual. Res* **18**, 1531–1544 (2018).
76. Liu, J. Y. *et al.* Association of ultrafine particles with cardiopulmonary health among adult subjects in the urban areas of northern Taiwan. *Sci. Total Environ.* **627**, 211–215 (2018).
77. Matsumoto, K., Takusagawa, F., Suzuki, H. & Horiuchi, K. Water-soluble organic nitrogen in the aerosols and rainwater at an urban site in Japan: implications for the nitrogen composition in the atmospheric deposition. *Atmos. Environ.* **191**, 267–272 (2018).
78. Su, J., Zhao, P. & Dong, Q. Chemical compositions and liquid water content of size-resolved aerosol in Beijing. *Aerosol Air Qual. Res* **18**, 680–692 (2018).
79. Guo, H. B. *et al.* Size-resolved particle oxidative potential in the office, laboratory, and home: evidence for the importance of water-soluble transition metals. *Environ. Pollut.* **246**, 704–709 (2019).
80. Van Vaeck, L. & Van Cauwenberghe, K. A. Characteristic parameters of particle size distributions of primary organic constituents of ambient aerosols. *Environ. Sci. Technol.* **19**, 707–716 (1985).

81. Huang, Z. *et al.* Field intercomparison of filter pack and impactor sampling for aerosol nitrate, ammonium, and sulphate at coastal and inland sites. *Atmos. Res.* **71**, 215–232 (2004).
82. Pindado, O. *et al.* Characterization and sources assignment of PM 2.5 organic aerosol in a rural area of Spain. *Atmos. Environ.* **43**, 2796–2803 (2009).
83. Gietl, J. K. & Klemm, O. Source identification of size-segregated aerosol in Münster, Germany, by factor analysis. *Aerosol Sci. Tech.* **43**, 828–837 (2009).
84. Plaza, J., Pujadas, M., Gómez-Moreno, F. J., Sánchez, M. & Artiñano, B. Mass size distributions of soluble sulfate, nitrate and ammonium in the Madrid urban aerosol. *Atmos. Environ.* **45**, 4966–4976 (2011).
85. Frka, S., Grgić, I., Turšič, J., Gini, M. I. & Eleftheriadis, K. Seasonal variability of carbon in humic-like matter of ambient size-segregated water soluble organic aerosols from urban background environment. *Atmos. Environ.* **173**, 239–247 (2018).
86. Moya, M., Castro, T., Zepeda, M. & Baez, A. Characterization of size-differentiated inorganic composition of aerosols in Mexico City. *Atmos. Environ.* **37**, 3581–3591 (2003).
87. Miguel, A. H. *et al.* Seasonal variation of the particle size distribution of polycyclic aromatic hydrocarbons and of major aerosol species in Claremont, California. *Atmos. Environ.* **38**, 3241–3251 (2004).
88. Sardar, S. B., Fine, P. M. & Sioutas, C. Seasonal and spatial variability of the size-resolved chemical composition of particulate matter (PM 10) in the Los Angeles basin. *J. Geophys. Res.-Atmos.* **110**, D07S08 (2005).
89. Lough, G. C. *et al.* Emissions of metals associated with motor vehicle roadways. *Environ. Sci. Technol.* **39**, 826–836 (2005).
90. Chuaybamroong, P., Cayse, K., Wu, C. Y. & Lundgren, D. A. Ambient aerosol and its carbon content in Gainesville, a mid-scale city in Florida. *Environ. Monit. Assess.* **128**, 421–430 (2007).
91. Zhang, L. *et al.* Characterization of the size-segregated water-soluble inorganic ions at eight canadian rural sites. *Atmos. Chem. Phys.* **8**, 7133–7151 (2008).
92. Urban, R. C. *et al.* Sugar markers in aerosol particles from an agro-industrial region in Brazil. *Atmos. Environ.* **90**, 106–112 (2014).

Acknowledgements

The authors acknowledge support from NASA grant 80NSSC18K0148.

Author contributions

C.S. organized the dataset and led the conception and writing of the manuscript. All authors contributed to field data collection and quality control of dataset. C.S. conducted a final round of quality control on all datasets. All authors helped in the editing of the manuscript.

Competing interests

The authors declare no competing interests.

Additional information

Correspondence and requests for materials should be addressed to A.S.

Reprints and permissions information is available at www.nature.com/reprints.

Publisher's note Springer Nature remains neutral with regard to jurisdictional claims in published maps and institutional affiliations.



Open Access This article is licensed under a Creative Commons Attribution 4.0 International License, which permits use, sharing, adaptation, distribution and reproduction in any medium or format, as long as you give appropriate credit to the original author(s) and the source, provide a link to the Creative Commons license, and indicate if changes were made. The images or other third party material in this article are included in the article's Creative Commons license, unless indicated otherwise in a credit line to the material. If material is not included in the article's Creative Commons license and your intended use is not permitted by statutory regulation or exceeds the permitted use, you will need to obtain permission directly from the copyright holder. To view a copy of this license, visit <http://creativecommons.org/licenses/by/4.0/>.

The Creative Commons Public Domain Dedication waiver <http://creativecommons.org/publicdomain/zero/1.0/> applies to the metadata files associated with this article.

© The Author(s) 2020